EFDA–JET–CP(10)05/20

M. Groth, G.D. Porter, M.E. Rensink, T.D. Rognlien, S. Wiesen, M.Wischmeier, T. Eich, A. Herrmann, S. Jachmich, C.J. Lasnier, H.W. Müller, J.G. Watkins, M.N.A. Beurskens, B.D. Bray, S. Brezinsek, N.H . Brooks, M.E. Fenstermacher, C. Fuchs, A. Huber, A. Kallenbach, A.W. Leonard, A. Meigs, D.L. Rudakov, the DIII-D and ASDEX Upgrade Teams and JET EFDA Contributors

Simulations of Divertor Particle and Heat Loads in Ohmic and L-mode Plasmas in DIII-D, AUG, and JET using UEDGE

Simulations of Divertor Particle and Heat Loads in Ohmic and L-mode Plasmas in DIII-D, AUG, and JET using UEDGE

M. Groth[1,2], G.D. Porter[2], M.E. Rensink[2], T.D. Rognlien[2], S. Wiesen[3], M.Wischmeier[4], T. Eich[4], A. Herrmann[4], S. Jachmich[5], C.J. Lasnier[2], H.W. Müller[4], J.G. Watkins[6], M.N.A. Beurskens[7], B.D. Bray[8], S. Brezinsek[3], N.H. Brooks[8], M.E. Fenstermacher[2], C. Fuchs[4], A. Huber[3], A. Kallenbach[4], A.W. Leonard[8], A. Meigs[7], D.L. Rudakov[9], and the DIII-D and ASDEX Upgrade Teams, and JET EFDA Contributors*

JET-EFDA, Culham Science Centre, OX14 3DB, Abingdon, UK

[1]Aalto University, Association EURATOM-Tekes, Otakaari 4, 02015 Espoo, Finland.
[2]Lawrence Livermore National Laboratory, 7000 East Avenue, CA 94550, USA.
[3]Forschungszentrum Jülich GmbH, EURATOM-Assoziation, TEC, Jülich, Germany.
[4]Max-Planck Institut für Plasmaphysik, EURATOM-Assoziation, Garching, Germany.
[5]Association 'Euratom-Belgian state', Ecole Royale Militaire, Brussels, Belgium.
[6]Sandia National Laboratories, Albuquerque, NM, USA.
[7]EURATOM/CCFE - Fusion Association, Culham Science Centre, Abingdon, UK.
[8]General Atomics, San Diego, CA, USA.
[9]University of California San Diego, La Jolla, USA.
** See annex of F. Romanelli et al, "Overview of JET Results", (Proc. 22 nd IAEA Fusion Energy Conference, Geneva, Switzerland (2008)).*

Preprint of Paper to be submitted for publication in Proceedings of the 19th International Conference on Plasma Surface Interactions, San Diego, California, USA. (24th May 2010 - 28th May 2010)

ABSTRACT

Measurements and simulations with the UEDGE code of radiated power, and ion saturation currents and power loads to the target plates have been compared for density scans in ohmic and low confinement mode plasmas in DIII-D, ASDEX Upgrade, and JET. Simulations including cross-field drifts and assuming elevated chemical sputtering yields of 3-4% move the numerical solutions closer to many of the measurements compared to omitting the drifts and using the published Davis-Haasz yields. Adopting these assumptions the simulations reproduce the measured currents and powers, and their functional dependence on upstream density to within a factor of 2, with the exception of the ion currents to the low field side target in ASDEX Upgrade and the high field side target in JET. The applicability of using enhanced sputtering yields is discussed by comparing measured and simulated emission from low charge state carbon in the divertor regions.

1. INTRODUCTION

Predictions of particle and heat loads to Plasma-Facing Components (PFCs) in future, nextstep fusion reactors presently rely on simulations with fluid edge codes [1], such as EDGE2D/EIRENE [2,3], SOLPS [4], and UEDGE [5]. To gain sufficient confidence in these predictions the physics models implemented in the codes must be thoroughly tested and validated against measurements from present tokamak devices. On the one hand, such task requires sufficiently complete sets of dependable experimental data taken over the range of plasma conditions to which the code is applicable. On the other hand, the uniqueness and robustness of the numerical solutions must be tested against assumptions of, e.g., the applied transport models and boundary conditions.

This paper describes detailed comparisons of measured and simulated divertor target particle and heat loads in quiescent ohmic and low confinement mode (L-mode) plasmas in DIII-D, ASDEX Upgrade (AUG), and JET using the fluid edge code UEDGE. This addresses validation of one single fluid edge code against measurements from tokamaks of significant different dimensions (DIII-D and AUG versus JET) and increasing divertor neutral compression (DIII-D $\rightarrow$ JET $\rightarrow$ AUG). Unlike EDGE2D/EIRENE and SOLPS, in UEDGE a fluid model is assumed for all neutral species as well as for all ion species. This paper continues previous efforts with UEDGE [6] and SOLPS [7] for DIII-D and AUG. In closing the loop, comparison and validation of EDGE2D/EIRENE and SOLPS simulations against subsets of the experimental data are described in other presentations at this conference [8,9].

2. EXPERIMENTAL DATA

A. Experimental setup

Particle and heat loads were measured in all three devices in lower single null, low-power ohmic (AUG) and L-mode plasmas (DIII-D, JET) with the ion gradient drift ($B\times\nabla B$) toward the divertor. In DIII and AUG, the core plasma density, normalized to the Greenwald density (n_{GW}) [10], was raised by discharge from 0.2 to 0.4 and 0.2 to 0.5, respectively. In JET, the core plasma density

was raised step-wise during a single discharge from n_{GW} of 0.2 to 0.4. The range in collisionality achieved in the electron channel is 5 to 50; for the ions about a factor of 2 lower due to higher ion temperatures. Resulting from the increase in density, the total heating power (ohmic and neutral beam heating) increased via resistive ohmic heating from 1.0MW to 1.2MW in DIII-D, 0.7MW to 1.0MW in AUG, and 2.8-3.0MW in JET. Concomitantly, the radiated power fraction (i.e., the total radiated power normalized to the total input power), rose from 0.4 to 0.9 in DIII-D, 0.3 to 0.8 in AUG, and 0.3 to 0.5 in JET. Spatially resolved target ion flux profiles were obtained by sweeping the High Field Side (HFS) and Low Field Side (LFS) strike points a few centimeters over Langmuir probe arrays embedded in the targets.

The three tokamaks differ in physical dimensions, main chamber material, neutral compression, and pumping conditions. DIII-D is medium-size device of major radius $R_{maj} = 1.7$ m and minor radius $R_{min} = 0.6$ m. Its PFCs are carbon (fine grain ATJ graphite) and, at the time of the measurements in 2004, it had an open divertor structure (with respect to escaping neutrals) and horizontal targets in the bottom of the device. The density scan was accomplished by deuterium gas injection into the main and divertor chambers and pumping by the vessel walls only, i.e., no cryo pumping. AUG is a medium-size tokamak ($R_{maj} = 1.7$m / $R_{min} = 0.5$m) with a closed divertor structure and vertical targets. At the time of the experiments, the PFCs in main chamber were (primarily) tungsten-coated tiles, while the divertor targets were made of carbon (fine grain graphite SGL R6710). Higher core plasma densities were achieved by deuterium injection into the divertor chamber and simultaneously pumping by both the divertor cryo pump and the vessel walls. JET is a large-size tokamak ($R_{maj} = 3.0$ m / $R_{min} = 0.9$ m) with PFCs made of carbon-fiber composite. The divertor geometry is less closed as in AUG, and an asymmetric divertor plasma configuration with the HFS strike point on the vertical divertor plate, and the LFS strike point on the horizontal plate was investigated in these studies. Deuterium gas was injected from the main chamber and pumped by both the divertor cryo pump and the vessel walls.

For all three devices, the total radiated power (P_{rad}), and the ion saturation current (I_{div}) and power (P_{div}) to the HFS and LFS divertor targets were measured with bolometry, Langmuir probes, and infrared cameras, respectively. These parameters were calculated from spatially distributed line-of-sight measurements of the total radiation in both the main and divertor chambers, and the radial profiles of the ion saturation current density (j_{sat}) and the power density (q_{div}) along the HFS and LFS targets. Integration in the radial and toroidal direction yields the total target ion current and power.

B. Functional dependence of Idiv and Pdiv with upstream density

The measured I_{div} to the target plates shows that attached, high-recycling, and detached divertor plasmas were achieved in DIII-D and AUG, and attached and high-recycling divertor plasmas in JET. The dependences of $P_{rad,SOL}$ (the total radiated power within the SOL) with upstream density, n_{up}, is shown in Fig. 1 for the three devices. The upstream electron density at the separatrix, $n_{e,sep}$,

is used in Figs. 1 – 3 to describe n_{up}. In DIII-D and AUG, I_{div} to the HFS divertor plate successively decreases to zero as the upstream density, n_{up}, is raised (Fig. 2a,c), whereas I_{div} to the LFS divertor plate peaked at intermediate n_{up}, and decreased as n_{up} was further increased (Fig. 2b,d). Both observations demonstrate that (a) the HFS divertor plasma was partially detached already at the lowest n_{up}, and fully detached at the highest n_{up}; (b) the LFS divertor plasma went from being attached to being high-recycling at intermediate n_{up}, and to being detached at the highest n_{up}. In JET, I_{div} to both the HFS and LFS target increased with n_{up}, and no maximum current or reduction of I_{div} was observed (Fig. 2e,f). In DIII-D and JET P_{div} to the HFS and LFS target plates decreased continuously as nup was raised (Figs. 3a,b and Figs 3e,f), whereas in AUG P_{div} to both target plates slightly increased with increasing n_{up} (Figs. 3c,d). One may speculate that the lower P_{rad} measured in AUG compared to DIII-D, and the directly proportional dependence of P_{div} with n_{up} in AUG is related to the difference in main chamber PFCs between the two devices. Any further interpretation is beyond the scope of this paper.

3. UEDGE SIMULATIONS OF THE DENSITY SCAN IN DIII-D, AUG, AND JET

A. UEDGE setup

The density scans in DIII-D, AUG, and JET were simulated with the 2-D multi-fluid plasma, multi-fluid neutral edge code UEDGE, including E×B and B×∇B cross-field drifts [11], post-processed for P_{rad}, I_{div}, and P_{div}, and compared to the experimental data. Similar as possible assumptions on plasma transport and boundary conditions were made in the simulations for all three devices, and systematically varied to account for differences in the device setup (e.g., main chamber PFCs and pumping conditions) and measured upstream conditions (e.g., input power, density and temperature profiles). Non-orthogonal computational grids were used to better approximate the actual divertor target geometries. The effect of cross-field drifts was investigated by running scans without and with these terms activated. In UEDGE, plasma transport in the parallel-B direction is modeled using the Bragiinski equations, including limiters to constrain the fluxes to 21% of the free-streaming flux. In the radial direction a purely diffusive model with radially varying transport coefficients is assumed, modeled to match the measured upstream profiles of n_e and T_e, and ion temperature (T_i). Radial diffusion coefficients of 0.5 to 1.0 m^2/s were typically assumed for the innermost grid cells, 0.1 to 0.2 m2/s just inside and outside the separatrix, and 1 to 10 m2/s in the far SOL to match the measured ne profiles. Radially increasing heat diffusivities between 0.2 and 2.0 m^2/s were assumed for the electrons to match the measured T_e profiles, and a radially constant heat diffusivity of 0.75 m^2/s for the ions was chosen due to the scarcity of T_i measurements. Neutral transport within the computational domain is described by fluid continuity and momentum equations [12]. Deuterium ions striking the divertor plates are recycled as neutral atoms with 100% efficiency, whereas deuterium neutrals striking the plates, the grid boundary facing the Private Flux Region (PFR), and the outermost grid boundary in the main SOL are recycled with 99% efficiency. To account for divertor cryo pumping in AUG a neutral recycling efficiency of 95% was imposed at the PFR grid boundary, while for

JET (and this study) an efficiency of 99% was assumed. Carbon releasedby physical and chemical sputtering at the plates and by chemical sputtering at the walls isemitted from the surface using the Davis-Haasz rates [13] into the computational domain asneutral carbon. The carbon injection rates are defined via lookup tables for a given target temperature (here, 300 K) and impact energy of the deuterons at each wall segment. The resulting chemical sputtering yields, Y_{chem}, typically vary between 0.5% and 3%. Spatially constant multipliers (f_{Ychem}) are used to modify Y_{chem}. Carbon transport and ionization are modeled using a force balance equation in the parallel-B direction, and diffusion in the radial direction with the same transport coefficients as for the deuterons, and collisional ionization, recombination, and charge exchange rates from ADAS [14].

An initial set of transport and recycling coefficients and f_{Ychem} equal to unity were assumed to match the upstream profiles of lowest density case, and then held constant for all higher densities. At simulated densities matching the experimental n_e profiles, the total power across the innermost grid boundary was raised until it reproduced the measured total heating power. Further refinement of the electron heat diffusivity profiles was performed, if necessary, until the simulated and measured T_e profiles match. This procedure was repeated for cases without and with cross-field drifts, and for all three devices.

B. Comparison of measured and simulated P_{rad}, I_{div}, and P_{div}

Including cross-field drifts and assuming twice the published chemical sputtering reproduces the measured total radiation in the SOL for all three devices, whereas the no-drift and $f_{Ychem} = 1$ cases show 50% lower radiated power at the highest densities (Fig. 1). Inclusion of cross-field drifts typically increases $P_{rad,SOL}$ by 10% to 20%, as a result of higher densities yielded in the HFS divertor plasma over the no-drift case, while doubling Y_{chem} ($f_{Ychem} = 2$) results in a 15% to 40 % increase in $P_{rad,SOL}$ due to elevated carbon levels. In simulations pertaining to DIII-D, the upstream density limit, at which the temperature in the LFS X-point region drops below 5 eV, is also obtained at 20% lower n_{up}.

For all three devices, the ion current to the HFS target decreases with increasing n_{up}, as observed experimentally in DIII-D and AUG, when cross-field drifts are included and $f_{Ychem} = 2$ is assumed (Fig.2). Without drifts, $I_{div,HFS}$ saturates at 30% lower n_{up} (DIII-D) or does not saturated at all (AUG). The simulations for JET with drifts and $f_{Ychem} = 2$ predict an inversedependency with n_{up} as seen experimentally. At the LFS target, inclusion of drifts in the simulations for DIII-D results in the experimentally observed saturation of I_{div}, but at approximately twice the measured current. In the AUG simulations, I_{div} to the LFS target steadily increases with increasing n_{up} until the density limit is reached, and saturation of I_{div} as seen in the experiment is not observed. Including drifts and assuming $f_{Ychem} = 2$ reduce the current by a factor of 2 at the density limit. Assuming constant input power (2.2 MW) and $f_{Ychem} = 2$ in the JET simulations, I_{div} to the HFS target steadily decreases until the density limit is reached, while at the LFS target I_{div} increases with increasing n_{up}. At onset of detachment of both the HFS and LFS divertor plasma, $I_{div,HFS}$ sharply increases and $I_{div,LFS}$ abruptly

decreases, indicating cross-talk between the two divertor legs across the PFR.

Raising n_{up} and adjusting the input power at the domain core boundary to the power measured experimentally lead to a reduction of P_{div} to the HFS target in the simulations pertaining to DIII-D and JET, while for AUG P_{div} remains almost constant (Fig. 3). For DIIID, $P_{div,HFS}$ decreases by a factor of 2, approximately, when drifts are included and f_{Ychem} is set to 2, moving the simulations closer to the experimental data. For AUG, the simulated $P_{div,HFS}$ brackets the measurements, for which the no-drift case assuming $f_{Ychem} = 2$ comes closest to the experimental data. The drift case with $f_{Ychem} = 2$ reproduce the measured $P_{div,HFS}$ for JET. At the LFS target, P_{div} decreases (DIII-D), and remains constant or increases (AUG, JET) with increasing upstream n_{up}. The simulations for DIII-D overestimate the measurements by 75% at the lowest n_{up}, and including drifts and assuming $f_{Ychem} = 2$ show the steepest decline in $P_{div,LFS}$ with nup, in agreement with the experimental data. For AUG, the simulations assuming $f_{Ychem} = 1$ reproduce the measured increase of $P_{div,LFS}$ with n_{up}, for cases without or with drifts. For JET, $P_{div,LFS}$ increases with nup, and remains constant when drifts are included and $f_{Ychem} = 2$ is assumed. For constant input power and $f_{Ychem} = 2$, $P_{div,LFS}$ decreases and sharply drops as the HFS and LFS divertor plasmas detach.

4. DISCUSSION

Simulations of ohmic and L-mode density scans in DIII-D, AUG, and JET with UEDGE commonly show that an agreement between the measured and simulated parameters $P_{rad,SOL}$, I_{div}, and P_{div} within a factor of 2, or better, can be achieved when drifts are included and enhanced chemical sputtering yields of Davis-Haasz [13] are assumed. This conclusion particularly applies to $P_{rad,SOL}$ in all three devices, as well as for $I_{div,LFS}$ and $P_{div,LFS}$ to the HFS target in DIII-D, $I_{div,LFS}$ to the HFS in AUG, and $P_{div,LFS}$ to the LFS in JET. The most significant disagreement are obtained in the simulations for DIII-D for $I_{div,LFS}$ and $P_{div,LFS}$, in which both the predicted currents and powers overestimate the measurements by a factor of 2; for AUG and $I_{div,LFS}$, in which no saturation of I_{div} was obtained below the density limit; and for JET and $I_{div,HFS}$, in which the measured and simulated currents show opposite functional dependences on n_{up}. It is worth noting that for AUG, the simulations with drifts and $f_{Ychem} = 2$ better reproduce the I_{div} dependence at the HFS plate, but setting $f_{Ychem} = 1$ produces the better match for P_{div} to both the HFS and LFS targets.

Comparisons of the measured and simulated emission profiles of low charge state carbon in the divertor do not conclusively confirm or dismiss the assumption of enhanced chemical sputtering, in particular at the HFS target plates. While the simulations with $f_{Ychem} = 2$ for the density range investigated for DIII-D overestimate the peak emission of neutral carbon (CI 910 nm) and doubly ionized carbon (CIII 465 nm) by factors of 2 to 3, they significantly better reproduce (within 50%) the emission from singly ionized carbon (CII 515 nm). Similarly, simulations of the lowest density case in AUG better reproduce the CIII emission (465 nm) measured in both the HFS and LFS divertor regions when $f_{Ychem} = 2$ is assumed, and the CI (910 nm) and CII (515 nm) for the high-recycling conditions in JET. Hence, besides uncertainties in the measured photon fluxes and assumption of

Y_{chem}, simulating the 2-D distribution of the divertor background plasma and carbon transport may also be an issue.

Better agreement between measured and simulated plasma and emission parameters can be achieved by assigning spatially varying Y_{chem} to the HFS and LFS target plates. This may be justified, as carbon surface layers observed in tokamaks yield higher Y_{chem} [15]. On the other hand, the applied Davis-Haasz Y_{chem} do not include the flux dependence measured by Roth et al. [16] and may generally differ by factors of 2, or more, under certain conditions.

However, in assigning spatially varying Y_{chem} one may conceal the fact that other physics besides chemical sputtering is inadequately modelled. These deficiencies include using diffusive radial transport models and underestimating recycling and impurity production at the main chamber walls, main chamber materials, neutral pumping at the targets, and neutralplasma interaction and molecular physics. As examples, to account for tungsten as the main chamber material in the simulations for AUG, reducing f_{Ychem} for $Y_{chem,carbon}$ at the main wall from 1.0 to 0.1 does not affect $P_{rad,SOL}$ at the lowest n_{up}, but lowers $P_{rad,SOL}$ by 15% at the highest n_{up}, thus moves the simulations away from the experimental data. Enhanced sputtering due to intermittent radial transport is expected to increase the effect on P_{rad}, and subsequently on I_{div} and P_{div}, in particular at high n_{up}. Likewise, lowering the recycling coefficient for neutrals at the PFR grid boundary in the JET simulations to increase the pumping efficiency, reduces $I_{div,LFS}$ and increases $P_{div,HFS}$, thus moves the numerical solutions away from the experiment. Unfortunately, addressing these issues more thoroughly in this paper is beyond its scope.

ACKNOWLEDGMENT

This work was performed in part under the auspices of the U.S. Department of Energy by Lawrence Livermore National Laboratory under Contract DE-AC52-07NA27344, DE-FG02- 07ER54917, DE-AC05-00OR22725 and DE-AC04-94AL85000. This work was also supported by EURATOM and carried out within the framework of the European Fusion Development Agreement (EFDA). The views and opinions expressed herein do not necessarily reflect those of the European Commission. The project was co-funded via an EFDA Fellowship in Fusion Research 2009-2010.

REFERENCES

[1]. A.S. Kukushkin et al., Nuclear Fusion **49** (2009) 075008.
[2]. A. Taroni et al., Contribution Plasma Physics **32** (1992) 438.
[3]. S. Wiesen et al., www.eirene.de/e2deir_report_30jun06.pdf.
[4]. R. Schneider et al., Contribution Plasma Physics **46** (2006) 3.
[5]. T.D. Rognlien et al. J. Nuclear Material **196-198** (1992) 347.
[6]. M. Groth et al., Proceedings of the 2007 EPS conference, P1.039, Warsaw, Poland.
[7]. M. Wischmeier et al., J. Nuclear Material **390-391** (2009) 454.
[8]. S. Wiesen et al., this conference.

[9]. M. Wischmeier et al., this conference.
[10]. M. Greenwald et al., Nuclear Fusion **28** (1988) 2199.
[11]. T.D. Rognlien et al., Journal of Nuclear Materials **266-269** (1999) 654.
[12]. T.D. Rognlien et al., Contribution Plasma Physics **36** (1996) 105.
[13]. J.W. Davis, A.A. Haasz Journal of Nuclear Materials **241-243** (1997) 37.
[14]. Atomic Data and Analysis Structure 1995-2008, http://adas.phys.strath.ac.uk.
[15]. S. Brezinsek et al., Journal of Nuclear Materials **337-339** (2005) 1058.
[16]. J. Roth et al., Nuclear Fusion **44** (2004) L21.

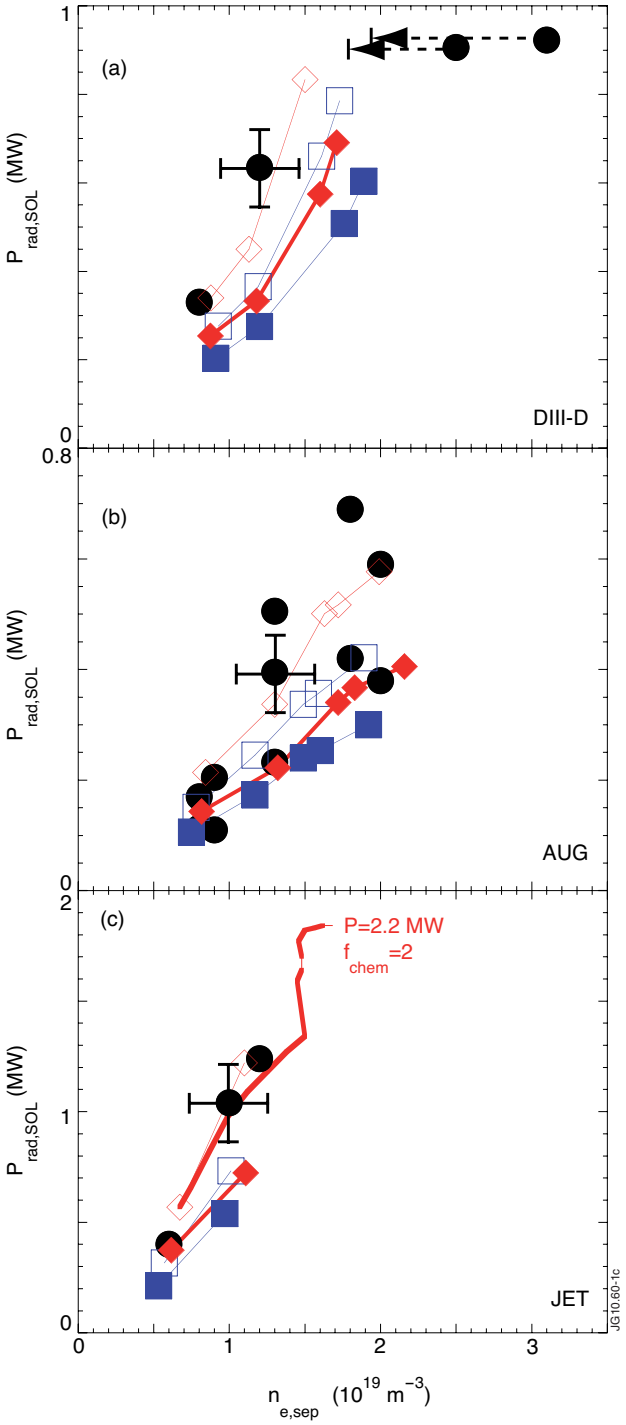

Figure 1: Total radiated power from the SOL ($P_{rad,SOL}$) as measured by bolometry and simulated by UEDGE for (a) DIII-D, (b) AUG, and (c) JET plotted as function of upstream (LFS midplane) electron density at the separatrix ($n_{e,sep}$). The experimental data are given by the black solid circles. Simulation results are shown for cases without (blue squares) and with (red diamonds) inclusion of cross-field drifts, and f_{Ychem} =1 (solid symbols) and f_{Ychem} =2 (open symbols). The uncertainty in the measured $n_{e,sep}$ and $P_{rad,SOL}$ is indicated by the double cross. For DIII-D and the two highest $n_{e,sep}$, a 1cm outward shift of the upstream n_e profile would result in a 50% reduction of $n_{e,sep}$ (as indicated by the two arrows), which is within the uncertainty of the magnetic equilibrium reconstruction.

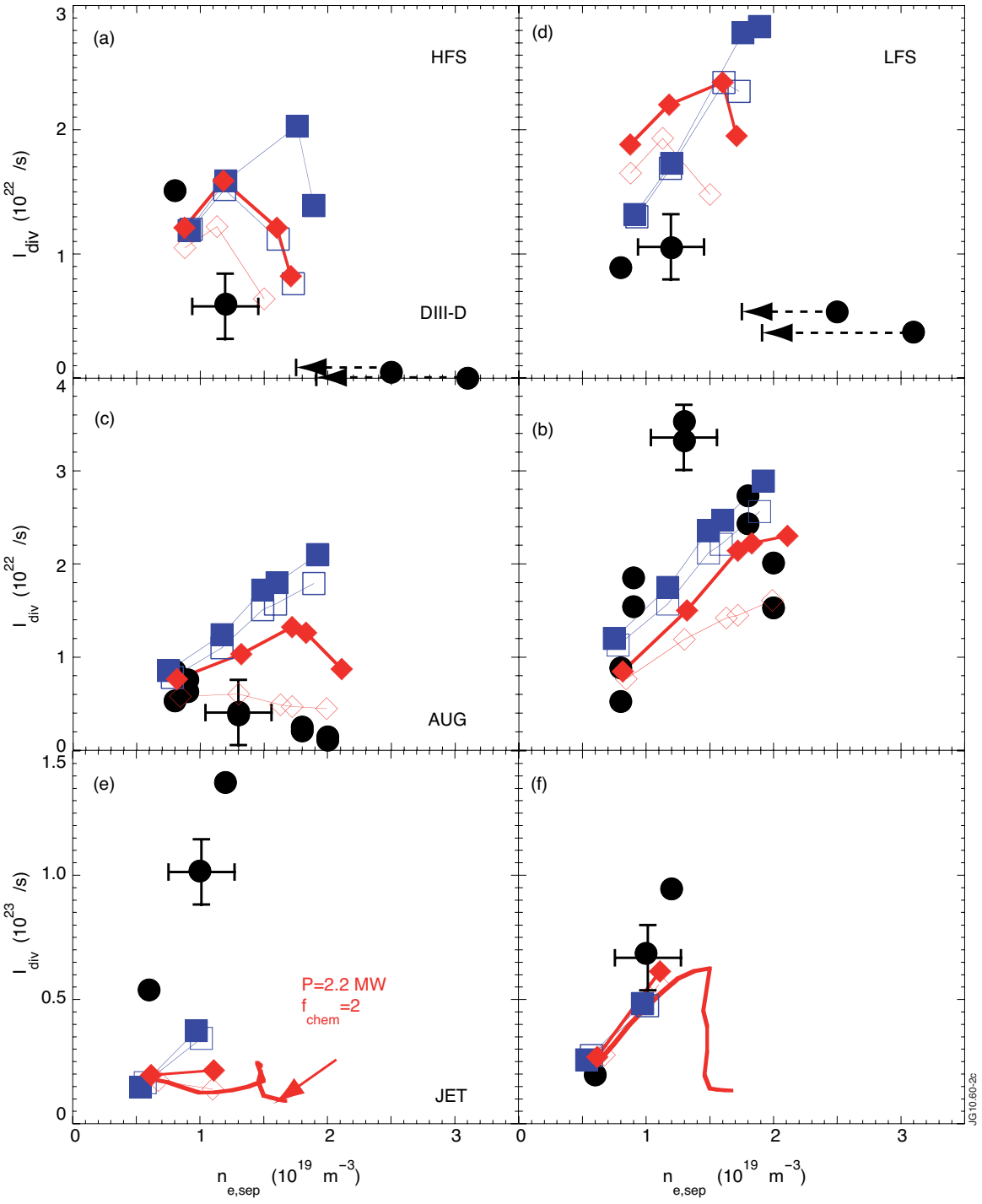

Figure 2: Langmuir probe ion current to the HFS (a,c,e) and LFS (b,d,f) targets for DIII-D (a, b), AUG (c,d), and JET (e, f) as a function of $n_{e,sep}$. Symbol style and color coding as in Figure 1.

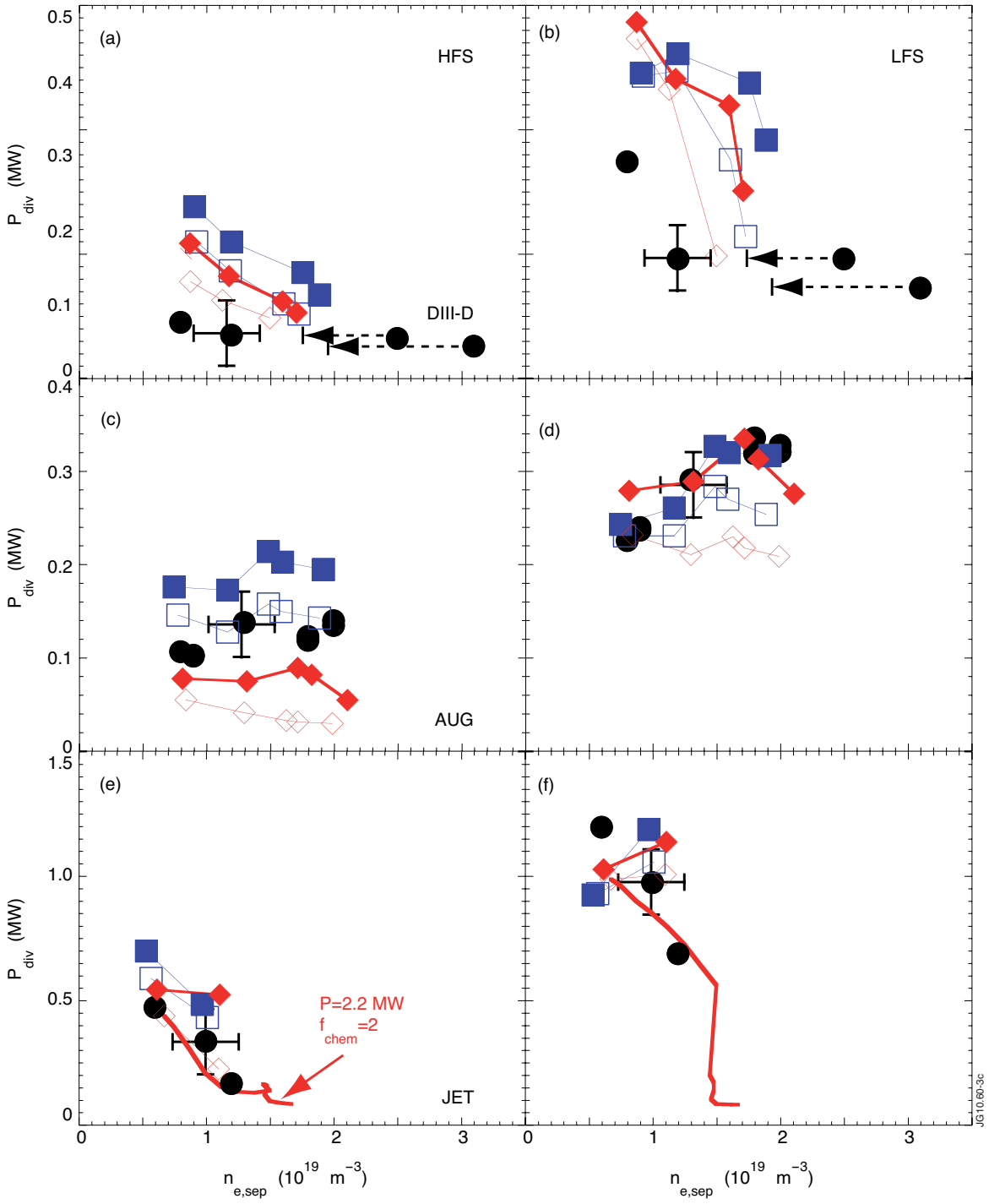

Figure 3: Infrared camera power to the HFS (a,c,e) and LFS (b,d,f) targets for DIII-D (a, b), AUG (c,d), and JET (e,f) as a function of $n_{e,sep}$. Symbol style and color coding as in Figure 1.